FLUID MECHANICS RESEARCH LABORATORY

FMRL TR-1

The Development of Laser Speckle or Particle Image Displacement Velocimetry. Part I: The Role of Photographic Parameters

by

L.M.M. Lourenco and A. Krothapalli

FAMU/FSU College of Engineering
Department of Mechanical Engineering
The Florida State University
Tallahassee, Florida 32306

May 1985

* C-4

ACKNOWLEDGMENTS

The support of NASA Ames Research Center for this work, under grant no. NAG 2-314 is greatly appreciated. The timely discussions with Dr. C.A. Smith of NASA Ames were very helpful in conducting these experiments. Most of the data analysis was carried out at the Von Karman Institute for Fluid Dynamics in Brussels. Our thanks to Professors M.L. Riethmuller and J.M. Buchlin from VKI for their help.

The collaboration of Drs. George Buzyna, Robin Kung and Mr. Michael Evans of Geophysical Fluid Dynamics Institute is fully acknowledged. The experimental set-up was expertly designed by Mr. Lew Eckhart.

Table of contents:

1. INTRODUCTION

One of the difficult problems in experimental fluid dynamics remains the determination of the vorticity field in fluid flows. The difficulty arises from the fact that vorticity is a quantity defined in terms of local velocity gradients and the available velocity measurement techniques e.g. Laser Doppler Velocimetry and Hot Wire Anemometry, are only sensitive to the local flow velocity. Current methods for vorticity measurements use multiple probes to independently measure one or more components of the velocity vector at two closely spaced spatial locations, from which a vorticity value is inferred by applying some kind of finite difference scheme (1,2). These methods suffer from some drawbacks. Firstly, when Hot-Wire probes are used, the local flow vorticity may be strongly influenced due to non-negligible blockage effects caused by the multiple probes. Secondly, the location of each individual measuring probe volume (LDV and HW alike) may not be spatially close enough to resolve and accurately measure the local velocity gradients. As a consequence the measured vorticity is only a "spatially filtered" estimate of the actual vorticity field. Another important aspect that needs to be considered is that these techniques can only provide "one point" information. In order to obtain whole field data, measurements must be carried out sequentially one point at a time. Although this sequential method can be easily implemented in applications involving steady flows, it is of rather difficult application in unsteady flow phenomena.

Recently, a novel velocity measurement technique, commonly known as Laser Speckle or Particle Image Displacement Velocimetry became available (3-7). This technique permits the simultaneous visualization of the two-dimensional streamline pattern in unsteady flows and the quantification of the velocity field.

The main advantage of this new technique is that the whole two-dimensional velocity field can be recorded with great accuracy and spatial resolution, from which the instantaneous vorticity field can be easily obtained. This constitutes a great asset for the study of a variety of flows that evolve stochastically in both space and time, and in the case of interest, to the study of unsteady vortical flows which occur in rotorcraft and in high angle of attack aerodynamics.

2. PRINCIPLE OF THE TECHNIQUE

The application of Laser Speckle or Particle Image Displacement Velocimetry to fluid flows followed the use of Laser Speckle methods in solid mechanics, in which object displacement and rotation were accurately measured (8).

When applied to the measurement of fluid flows the technique involves two equally important steps. In the first step a selected plane of the flow field is recorded. Similarly to Laser Doppler Velocimetry the flow is seeded with small tracer particles. A sheet of coherent light is used to provide a "surface" within the fluid. A pulsed laser such as a Ruby or a NdYag laser, or a CW laser with a shutter device is normally used as the light source. The laser sheet is formed, for example, by focusing the laser beam first with a long focal length spherical lens, to obtain minimum thickness, and then diverging the beam in one dimension with a cylindrical lens (Fig. 1). The light scattered by the seeding particles in the illuminated plane provides a moving pattern. When the seeding concentration is low, the pattern consists of resolved diffraction limited images of the particles. When their concentration increases, the images overlap and interfere to produce a random speckle pattern. A multiple exposure photograph records this moving pattern.

In a second step the local fluid velocity is derived from the ratio of the measured spacing between the images of the same tracer, or speckle grain, and the time between exposures. The recorded image formed by isolated Airy disks, in the cases of low seeding concentration, or speckle grains for high seeding concentration, is a complicated random pattern. In this image the local displacements can hardly be measured by visual or computer-aided inspection. Methods for the direct analysis of these images have been used but with limited success (9). The displacement measurements have an associated error which becomes important when the spacing between successive tracer images becomes small. This method also fails when the mean distance between tracers is of the same order of magnitude as the distance a tracer particle travels during the time between exposures. As a consequence the tracer concentration is usually kept small, resulting in velocity measurements with poor spatial density.

Alternative methods used in similar data analysis in solid mechanics are applicable and provide good results. Two methods are currently being

developed and investigated. These are the local coherent illumination to produce Young's fringes and local two-dimensional correlation of the image. In the first method, the diffraction produced by local coherent illumination of the multiple images in the photograph generates straight fringes in the Fourier plane of a lens. These fringes have an orientation which is perpendicular to the direction of the local displacement vector and a spacing which is inversely proportional to its magnitude (Fig. 2). The displacement vector is determined by the analysis of these fringe patterns. Amongst the various analysis methods being developed, Fourier and Autocorrelation techniques seem to be the most effective and accurate. In the two-dimensional correlation method a small area of the image being interrogated is digitized, in a NXN point format (where N is the number of pixel rows or columns), and a two-dimensional correlation is performed. This results in a digital autocorrelation function with a maxima at the coordinates corresponding to the average displacement of the tracers (Fig. 3). Basically this method is equivalent to the general Young's fringe method because the two-dimensional fourier transform of the fringe pattern is equal to the autocorrelation function. The major drawback of this method is that the computation of the autocorrelation function requires large data arrays and becomes extremely slow when N (number of pixel rows or columns) is large. A new processing method, proposed by Yao and Adrian (1Ø), reduces the general NXN element of a two-dimensional problem to two N element one-dimensional problems, by compressing the information in two orthogonal directions using integration techniques. Although attractive, this procedure leads to some loss of information. Therefore, what has to be balanced is this loss versus the gain in computational speed. Future plans in this research include a critical evaluation of each of the above mentioned methods. However, we believe that the image analysis using the Young's fringe method is the most promising approach.

2.1 Image Analysis Using the Young's Fringe Method

Consider the function D(x,y) describing the light intensity produced by the scatterers in the image plane of the photographic camera, where x,y are the plane coordinates. Considering that there is a in-plane displacement, dy, of the scatterers, the speckle or particle images will be translated by Mdy,

where M is the magnification of the camera lens. The resulting intensity distribution in the image plane becomes

$$D(x,y) + D(x,y+My) = D(x,y) \otimes [\delta(x,y) + \delta(x,y+My)] \quad (1)$$

where $\delta(x,y)$ is the Dirac delta function centered on x,y, and considering that a translation can be represented as a convolution with a delta function. The total intensity is recorded on a photographic plate. After development, the transmittance, Γ, of the negative is given by

$$\Gamma = a+b\, D(x,y) \otimes [\, \delta(x,y + My)] \quad (2)$$

where a and b are characteristic constants of the photographic emulsion.

Two-dimensional Fourier transformation of the image is efficiently performed by optical processing of the photographic negative. This is achieved by locally analyzing the film negative with a probe laser beam. This process produces, as explained in the following, a straight fringe pattern whose orientation and magnitude are related to the direction and magnitude of the displacement. The resulting Fourier transform of the transmittance distribution, Γ, is

$$\tilde{\Gamma}(u,v) = a\, \delta(u,v) + b\, \tilde{D}(u,v)\, [1 + \exp(i2\pi vMy/\lambda_a)] \quad (3)$$

where $\tilde{\Gamma}$ represents the Fourier transform of Γ, u and v are angular coordinates of a point in the Fourier plane of the lens, λ_a is the wavelength of the interrogating laser light beam.

The first term, a $\delta(u,v)$ on the r.h.s. of equation 3 represents the image of a point source, i.e. the interrogative beam, when diffraction effects are neglected. This image is seen as a small bright spot in the center of the Fourier plane (Fig. 2). The second term is composed of a diffraction pattern, characteristic of the speckle or particle images, modulated by $[1+\exp(i2\pi vMy/\lambda_a]$

The intensity distribution for the second term is obtained by multiplication with its complex conjugate, resulting in

$$|\tilde{D}(u,v)|^2\, [\, 4\, \cos^2(\, \pi vMy/\lambda_a)] \quad (4)$$

The diffuse background, $|\tilde{D}(u,v)|^2$ is modulated by a set of Young's fringes whose spacing is given by

$$d_F = \frac{\lambda_a f_L}{M dy} \tag{5}$$

where f_L is the focal length of the converging lens. Knowing M, f_L, λ_a and measuring d_F, the displacement dy is easily found from equation 5, with the direction of the motion perpendicular to the orientation of the fringes.

By scanning the multiple exposed photograph, one can resolve the two components of the displacement and derive the velocity vector at every point in the field. This is a unique capability of this technique.

2.1 Nature of the Present Research

The motivation for the present work is to determine and develop the necessary background for the use of Laser Speckle or Particle Image Displacement Velocimetry to study vortical unsteady flows.

In this phase of the work we report on the optimization of the photographic parameters involved in obtaining the multiple exposure photograph.

3. A GUIDELINE FOR THE CHOICE OF THE PHOTOGRAPHIC PARAMETERS INVOLVED IN A MEASUREMENT USING LASER SPECKLE (LSV) OR PARTICLE IMAGE DISPLACEMENT VELOCIMETRY (PIDV)

The parameters playing a role in velocity measurements using Laser Speckle or Particle Image Displacement Velocimetry are:

(i) Tracer: type, concentration and dimensions.

(ii) Exposure parameters: time between exposures, exposure time and number of exposures.

(iii) Film parameters: sensitivity, grain and resolution.

These parameters are interrelated and their choice depends upon several factors as follows: the flow field of interest, namely the velocity range and area of the flow to be recorded; the required spatial resolution and accuracy; available hardware such as type of laser, CW or pulsed, laser power and laser light wavelength, and on the camera used for the photography.

3.1 Tracer

Tracers to be used in a measurement involving LSV or PIDV have to be as small as possible to accurately follow the fluid motions, and good light scatterers. These requirements are usually met by tracers used in LDV applications. In liquid flows we recommend the use of pliolite particles, which are practically neutrally buoyant in water, latex and titanium dioxide. In air flows, oil smoke or fog produces a relatively uniform seeding.

As previously mentioned, the light scattered by the seeding particles can create, depending on the seeding concentration, two entirely different patterns. This originates two modes of operation of the technique. For low seeding concentrations, the pattern consists of resolved diffraction limited images of the particles. When this concentration increases, the images overlap and interfere in the image plane to produce a random speckle pattern. In either case, the pattern is recorded in a multiple exposed photograph from which the velocity data is obtained. However, in the Particle Image mode of operation, due to light seeding, regions of the flow field may be left unseeded, or with poor seeding, resulting in signal drop-out. On the other hand, in the Laser Speckle mode of operation, the drop-out problem is minimized but other more restrictive complications may occur, as described

below. These problems preclude the use of the Laser Speckle mode of operation in the majority of flow fields of interest.

The Laser Speckle mode of operation relies on the recording of identical laterally shifted speckle patterns. Slight out-of-plane motion of the scatterers, due to flow three-dimensionality, between the exposures results in speckle patterns that are not entirely similar. As a consequence, their correlation decreases and local coherent illumination does not produce Young's fringes, or produces fringes with poor contrast and signal to noise ratio (SNR). This poses a severe limitation in the use of the Laser Speckle Displacements for the measurement of velocity in turbulent flows, or flows with an important velocity component in the direction perpendicular to the measuring plane. The fringe quality becomes less dependent on the out-of-plane motion when individual particle images are imaged and recorded, i.e. in the Particle Image mode of operation. In this case the tolerance to out-of-plane motion is roughly equivalent to the width of the illumination sheet and focusing depth of field of the recording optics. In addition, the high concentrations required by the Speckle mode of operation cause multiple scattering effects which result in the spreading of the thin laser illuminating sheet. Furthermore, the high concentration of tracers may strongly influence the flow field.

In conclusion, for a successful measurement using this technique, there are practical bounds to seeding concentration (Fig. 4). The upper boundary for the seeding concentration being set by a value above which a speckle pattern is formed due to the interference of light scattered by the individual particles. If C_p is the particle concentration and ΔZ the width of the laser sheet, we obtain for the maximum concentration

$$\sqrt{\frac{1}{\Delta Z C_p}} \gg dp \qquad (6)$$

where dp is the particle diameter. Considering typical values for dp = Ø.Ø1mm and ΔZ = Ø.5mm we obtain $Cp \ll 5.10^{12}\ m^{-3}$.

The lower end for the seeding concentration can be determined by considering that, in order to have a valid measurement, a minimum number of particle image pairs must be present in the area scanned by interrogation beam. The case of having a single particle image pair in the interrogation area is an ideal one, because it yields fringes with optimum SNR (Fig. 2).

However, this situation can only be achieved by lightly seeding the flow, thus giving rise to the so-called drop-out problem. An interesting case occurs when only two particle pairs are present in the interrogation area. The corresponding diffraction pattern includes multiple equally intense fringe patterns due to cross interference of non-corresponding image pairs. In this case, the local displacement cannot be resolved (Fig. 5). Finally, as the number of particle image pairs in the interrogation area increases, the cross interference fringes become weaker in comparison with the "main fringe pattern" which reflects the local displacement (Fig. 6). The cross-interference fringes are sometimes designated as a "background speckle noise." Our experience shows that, for reasonable fringe quality, at least four particle image pairs need to be present in the interrogation area. This number can be somewhat relaxed if more than two exposures were used for the photography. Considering that these particles exist in the volume defined dy the width, ΔZ, of the laser sheet, scanned by the beam whose diameter is D, we obtain for the average concentration:

$$C_p = \frac{16}{\Delta Z \ \pi \ D^2} \simeq 10^{-11} \ m^{-3} \tag{7}$$

3.2 Exposure Parameters

The exposure parameters are chosen in accordance with the maximum expected velocity in the field and the required spatial resolution. The spatial resolution, which is equal to the cross sectional area of the interrogating laser beam, is dictated by the scales involved in the fluid motion and should be less than the smallest scale.

The time between exposures, T, is determined by the maximum permissible displacement of a particle such that a correlation is obtained when locally analyzing the film negative with the probe laser beam. A necessary condition to obtain Young's fringes requires that the distance between adjacent particle images be less than a fraction of the analyzing beam diameter. In practice the maximum permissible displacement that can be detected corresponds to the case when the fringe spacing, d_F, is larger than the diffraction limited spot size, d_s, of the interrogating optics. In analytical terms:

$$d_F = \frac{\lambda_a \ f_L}{M v_{max} T} > d_s = \frac{4 \ \lambda_a f_L}{\pi \ D} \tag{8}$$

where M is the magnification factor, D and λ_a are respectively the

interrogation beam diameter and laser light wavelength. We obtain for the time between exposures

$$T = \frac{\emptyset.5\ D}{M v_{max}} = \frac{1}{F} \tag{9}$$

v_{max} is the maximum expected velocity in the field, and F the frequency corresponding to the inverse of the period T. For practical purposes we use the constant Ø.5 instead of Ø.8 as it would be given by equation 9.

The exposure time, t, is a free parameter when a CW laser source is used together with a shutter. In previous applications (3-7) the exposure time has been kept as small as possible for minimum particle image size. In a later study, Lourenco (11) demonstrated that the duration of the exposure time can be of the same order of magnitude as the time between exposures.

For very short exposures the recorded particle images are identical to the diffraction limited particle images as the particles appear to be stationary during the exposure. For longer exposures the recorded images become streaks whose length is directly proportional to the exposure time. Coherent illumination of these images generates Young's fringes superposed on a diffraction pattern which depends on the streak length. In the limiting case of a very short exposure, the diffraction pattern is symmetric and has a circular shape (Fig. 2). When the exposure time is increased, small streaks are generated, and the diffracted light in the spectrum is concentrated in a band whose width is inversely proportional to the streak length (Fig. 7).

Because of the finite width of the diffraction pattern, the number of fringes, n_F, in the pattern becomes a function of the ratio between the streak separation to the streak length, l_s. In analytical terms:

$$n_F = \frac{dy}{l_s} + 1 \tag{1Ø}$$

For an accurate measurement of the fringe spacing, it is necessary to have a reasonable number of bright fringes. Usually five bright fringes give good results.

Another parameter determining the degree of accuracy with which the fringe spacing can be determined is the contrast and sharpness of the Young's fringes. If the number of exposures, N, is larger than two and the particles

are displaced by the same amount after each exposure, the sharpness of the interference fringes can be greatly improved.

For a multiple exposure, the function describing the light intensity of the point sources becomes

$$D(x,y) \circledast \sum_{n=\emptyset}^{N-1} \delta(x, y + nMdy) \tag{11}$$

resulting in an amplitude distribution of the transmittance of the negative in the Fourier plane of a lens, as follows:

$$|\tilde{D}(u,v)|^2 \left\{ N+2 \sum_{n=1}^{N-1} n \cos \left[(N-n)\ 2\ \pi M\ dy/\lambda_a \right] \right\} \tag{12}$$

For a number of exposures, N, equal to two a relation similar to equation 4 is obtained as expected.

Figure 8 displays the fringe width for multiple exposures, normalized with the corresponding width for a double exposure, versus the number of exposures. It is clearly seen that an optimum fringe width can be obtained with a limited number of exposures.

The sharpening of the fringes using a multiple exposure recording technique is of great advantage because it allows a very easy visual and qualitative "measurement" of the direction and spacing of the young's fringes. It also increases their signal to noise ratio. Note that this improvement in the signal to noise ratio is a result of the artificial increase in particle concentration due to the multiple exposure.

3.3 Choice of the Film and Laser Power Requirements

The technique relies on the ability to detect and record on photographic media the seeding particles images. The particle is a function of the scattering power of the particles within the fluid, the amount of light in the illuminating sheet, camera lens and film sensitivity at the wavelength of the illuminating laser light. Although the particle detection increases

proportionally with increasing power of the illuminating laser, it is of great importance to keep the laser power requirement to its minimum. An important reason for this limitation is economy as the main component in the cost of the apparatus is the laser source and its price increases very rapidly with the power delivered.

In this section, we suggest films to be used and the laser power required to expose these films.

To compensate for the limited illuminating laser power, the films used to record the particle images, are required to have good sensitivity, but without sacrificing film resolution. When good precision is necessary, films with a resolution of about 3ØØ line-pairs/mm and sensitivity from 25 to 125 ASA (Afga Ortho 25, Kodak Technical Pan 2415) are suitable for the use either with pulsed Ruby lasers ($\lambda \sim 7ØØnm$) or pulsed, frequency doubled, NdYag lasers and CW Argon-Ion lasers ($\lambda \sim 5ØØnm$). When a NdYag or a CW Argon-Ion laser are used more sensitive films may be used. A particular film, Kodak Royal-X Pan, 125Ø ASA, has excellent sensitivity in 4ØØ-6ØØnm range, and retains fairly good resolution (1ØØ line-pairs/mm).

Another parameter to be accounted for is the film grain. When illuminating the film negative to produce Young's fringes, the film's unexposed grains can introduce amplitude and/or phase changes into the wavefront of the analyzing laser beam and thus create additional noise. This noise has generally a frequency content which is in the same range as the Young's fringes. Therefore its elimination is difficult either from optical or digital filtering. Film grain cannot be totally eliminated and it will always be present in different degrees, especially in applications where fast film is used, to cope with low power density of the illuminating sheet. A method of solution as been proposed (6) by which this source of noise is considerably reduced. It consists of producing a positive copy by contact printing on a very high resolution fine grain film, for example holographic plates. The positive copy is analyzed in the same manner using the laser probe beam. Figures 9a) and 9b) display respectively the interference fringe patterns generated for the film negative and corresponding positive. A remarkable decrease in noise level is achieved. Another advantage of using this procedure is that the intensity of central zero order spot, due to the laser probe beam, is also decreased or eliminated.

Once the film is selected, the amount of laser power required for the

exposure can be computed. For a successful exposure of the photographic emulsion the energy scattered by a tracer particle and viewed through the camera lens has to be larger than the film sensitivity at the wavelength of the illuminating laser. It is customary to write this condition in the following analytical form:

$$\overline{E} = \int_{\Delta t} T dt > C E_o \tag{14}$$

where $\overline{E}$ is the mean exposure level for a single particle (J/m^2), T is the average intensity of the light scattered by a particle (W/m^2), $E_\emptyset$ is the film fog level and Δt is the exposure time. C is a constant between 1 and 1Ø. The fog level is defined as the exposure level below which the transmissivity of the film is independent of the incident intensity (Fig. 1Ø). The average intensity, T, of the light scattered by a single particle can be expressed in terms of (1Ø)

$$T = \frac{4}{\pi k^2 d_i^2} I_o \int_\Omega \sigma^2 \, d\Omega \tag{15}$$

where I_o is the intensity of the illuminating sheet (W/m^2), k is the illuminating laser light wavenumber, $\sigma = \underset{\sim}{s} \cdot \underset{\sim}{s}^*$ is the Mie parameter, the viewangle of the camera lens and d_i is the dimension of the diffraction limited particle image composed of two terms (1Ø), neglecting aberrations and grain noise, as follows

$$d_i = \sqrt{d_p^2 + d_e^2} \tag{16}$$

The first one being the particle diameter and the second one the edge spread caused by the limited response of the recording optics

$$d_e = 2.44 \, \lambda (1+M) F\# \tag{17}$$

with F# the camera objective F number.

When a pulsed laser is used the laser power required is simply determined from equation 14, considering that the particle is stationary during the exposure

$$I_o > \frac{CE_o(\pi K^2 d_i^2)}{4\int \sigma^2 d\Omega} \tag{18}$$

Considering that for a pulsed laser the pulse duration (= exposure time) is a fixed parameter, it is customary to express equation 18 in terms of energy per pulse, ε_o

$$\varepsilon_o > \frac{CE_o(\pi K^2 d_i^2)}{4\int \sigma^2 d\Omega} \tag{19}$$

The recommended value for the constant C is between 3 and 5 to compensate for film reciprocity effects caused by the very short exposure.

In applications involving the use of CW laser the exposure time is variable and considerably longer. In this case integration of equation 14 is somewhat more elaborate. For the sake of simplicity let us assume that the fluid motion, and hence the seeding particles displacement is unidimensional. Let r_o, r and u be respectively the initial position, current position and velocity of a tracer particle, in the film plane. The current particle position can be expressed as

$$r = r_o + u\,t \tag{20}$$

The exposure can be determined integrating equation 14 and considering two cases, $t < \frac{d_i}{u}$ and $t \geq \frac{d_i}{u}$

$$\overline{E} = \int_{\Delta t < \frac{d_i}{u}} T(r)dt = \begin{cases} T\,\dfrac{(r-r_o)}{u} & r_o < r \leq r_o + u.\,\Delta t \\ T\,\Delta t & r_o + u\Delta t < r \leq r_o + d_i \\ \dfrac{T}{u}(r_o - r + d_i + u\,\Delta t) & r_o + d_i < r \leq r_o + d_i + u.\,\Delta t \end{cases} \tag{21}$$

$$\overline{E} = \int_{\Delta t \geq \frac{d_i}{u}} T(r)dt = \begin{cases} T\,\dfrac{r-r_o}{u} & r_o < r \leq r_o + d_i \\ T\,\dfrac{d_i}{u} & r_o + d < r \leq r_o + d_i + u.\,\Delta t \\ \dfrac{T}{u}(r_o - r + 2d_i + u\,\Delta t) & r_o + d + u.\Delta t < r \leq r_o + 2d_i + u.\Delta t \end{cases}$$

The maximum exposure is obtained for exposure times larger or equal to $\frac{d_i}{u}$

Thus, for the whole field, the optimum exposure, is equal to d_i/V_{max} which results in the maximum exposure, without a significant reduction on the dynamic range of the technique, as shown in the following section.

The CW laser power required is given by,

$$I_o \geq \frac{CE_o(\pi K^2 d_i^2)V_{max}}{4 \int \sigma^2 \, d\Omega \, d_i} \tag{22}$$

Equation 19 shows that CW laser power required for a measurement increases with the flow velocity. This limitation does not apply to the case of a pulsed laser where the pulse duration is independent of the flow velocity.

4. VELOCITY DYNAMIC RANGE

In the following we will analyze the technique's abilities of resolving large velocity gradients in flow fields, i.e. its dynamic range. The dynamic range is defined as the largest velocity difference that can be detected in the flow field.

The low end of the dynamic range is determined by considering that for a measurement the spacing between the successive particle diffraction limited images or streaks is well resolved, i.e. do not collapse on each other. In analytical form

$$l_s = d_i + V.t < V.T \tag{23}$$

Considering that the time between exposures, T, is a function of the maximum velocity V_{max}, substituting $t \simeq o$ for a pulsed laser and, $t = \frac{di}{V_{max}}$ for a CW laser, yields the following expressions for the minimum velocity,

$$V_{min} = \frac{2\,M\,V_{max}d_i}{D} \qquad \text{pulsed laser} \tag{24}$$

$$V_{min} = \frac{2\,M\,V_{max}\,d_i}{D - 2\,M\,d_i} \qquad \text{CW laser} \tag{25}$$

The velocity difference $\Delta V = \frac{V_{max} - V_{min}}{V_{min}}$ is the velocity dynamic range and we obtain,

$$\Delta V = \frac{D}{2\,M\,d_i} - 1 \qquad \text{pulsed laser} \tag{26}$$

$$\Delta V = \frac{D - 2\,M\,d_i}{2\,M\,d_i} - 1 \qquad \text{CW laser} \tag{27}$$

The dynamic range increases with shorter pulse durations and is maximum in applications involving the use of a pulsed laser. Considering typical values for d_i = .Ø3mm, D = Ø.5mm and M = 1, we obtain for the dynamic range,

$$\Delta V \simeq 7.5 \qquad \text{pulsed laser} \tag{28}$$

$$\Delta V \simeq 6.5 \qquad \text{CW laser} \tag{29}$$

5. ACCURACY OF THE TECHNIQUE

The overall accuracy of the technique depends on the accuracies which can be achieved in the photographic procedure and processing techniques. In this report we only discuss the accuracy of the photographic recording. The sources of error are the lens aberrations and the limited film resolution, causing the position of the particles to be recorded with an inherent error, and the spurious contributions on the in-plane displacement recording by the out-of-plane motion.

In section 3.1 it was pointed out that out-of-plane motion was a severe limitation on the use of speckle in Fluid Dynamics applications. The reason for this limitation was that slight out-of-plane motion by the scatterers, between the multiple exposure, results in non-identical shifted patterns poorly correlated. To cope with this problem one operates in the Particle Imaging mode, where the particles are directly imaged and recorded. However, as shown in the following, out-of-plane motion may also contribute to considerable errors in the velocity measurement.

Let us consider the imaging system of figure 11 and the particle in position P_o within the laser sheet. Between exposures the particle moves to a position M_o, due to three-dimensional fluid motion. The components of the displacement vector are dx, dy, dz, with dx and dy, the in-plane and dz the out-of-plane components of the displacement. In the image plane the photographic plate records the position of the particle at P_L and M_L. The coordinates of these points are given by:

$$\left.\begin{matrix} -Mx \\ -My \\ d_o+d_L \end{matrix}\right\} P_L \qquad \left.\begin{matrix} -M(x+dx)\ (1+ dz/d_L) \\ -M(y+dy)\ (1+ dz/d_L) \\ d_o + d_L \end{matrix}\right\} M_L \qquad (30)$$

where second order terms have been neglected for simplicity.

The displacement $P_L M_L$, measured by means of Young's fringes is given by

$$dx_m = Mdx\ (1 + \frac{xdz}{dxd_L}) \qquad dy_m = Mdy\ (1 + \frac{ydz}{dyd_L}) \qquad (31)$$

and the measured displacement components referred to the object plane are

$$dx_o = dx + \frac{xdz}{d_L} \qquad dy_o = dy + \frac{ydz}{d_L}$$

The contribution of the out-of-plane displacement to the measured displacement is given by two parasite terms (xdz/d_L) and (ydz/d_L). The error produced by the out-of-plane motion while negligible in the neighborhood of the optical axis, increases linearly, and may become important, with the distance from the optical axis. The influence of the out-of-plane motion becomes particularly important when imaging the flow with short focal and wide angle objectives.

A relation can easily be found for the theoretical error in a measurement due to out-of-plane motion:

$$E_x = \frac{dz}{dx} \tan \psi x \qquad (33)$$

$$E_y = \frac{dz}{dy} \tan \psi y$$

where ψ_x and ψ_y are respectively semi-field angle components along the x and y axis respectively. Hence the error depends only on the ratio of the out-of-plane to in-plane component of displacement and the tangent of the semi-field angle. Figure 12 shows the theoretical relative error for various ratios of dz/dx and tan ψx.

6. VALIDATION OF THE TECHNIQUE

6.1 Experimental Configuration

In order to evaluate the present capabilities of the technique a bench-top experiment was performed. In view of the application of the technique to vortical flows, two flows that include important vortical motions were generated and recorded. Both flows were created by towing models in the reduced scale Fluid Mechanics Research Laboratory towing tank facility (Fig. 13). The first one consisted of the Karman vortex street generated by a cylinder with 10 mm in diameter, and the second one by the flow over a 60mm chord airfoil (NACA 0012), at a 30 degree incidence. Both models were towed with a velocity of 23.5 mm/sec. The fluid used in these experiments was water seeded with small, .004 mm in diameter, particles (TSI model 10087). The corresponding Reynolds numbers were 230 for the cylinder and 1400 for the airfoil. These flows are excellent test cases because they include large scale vortical motions and extreme velocity gradients. These extreme ngradients serve as a test to the technique's capabilities of providing information over a large velocity range.

A view of the laser sheet arrangement is also shown in figure 13. The laser beam from a 5 Watt Argon-Ion laser (Spectra-Physics series 2000) is steered and focused to a diameter of .3mm using an inverse telescope lens arrangement. A cylindrical lens, with a focal length of -6.35 mm, is used to diverge the focused beam in one dimension, creating a light sheet. The laser sheet is 70 mm wide and illuminates the mid-span section of the models.

For the multiple exposure, the CW laser beam is modulated using a Bragg cell. This shutter has been assembled using standard equipment. A schematic is shown on figure 14. The advantages in using this shutter arrangement are the possibility of an independent choice of the number of exposures, the time between exposures and the exposure time.

Due to conditioning optics and Bragg cell losses, the available laser power was reduced to 70% of the total power. In this experiment the laser delivered 8 Watts in the multiline mode. The power density, I_o, of the laser sheet was

$$I_o = \frac{I}{d_b \, \Delta Z} = .27(W/mm^2) \tag{34}$$

with d_b ΔZ the laser sheet cross section, where d_b = .3 mm is the width of the focused laser beam, and ΔZ = 70 mm the laser sheet span.

The recording optics consisted of a 4x5" format camera with interchangeable objective lens. In this experiment we used a 135 mm lens. The lens aperture was set at F# 5.6 and the magnification factor was 0.47. The camera was positioned in the laboratory reference frame. Therefore, the flow field was recorded in the reference frame moving with the mean flow. The film used was a KODAK technical pan 2415 with a sensitivity of 125 ASA. This film has a resolving power of 320 line-pairs/mm and extremely fine grain. The large resolving power is required for increased recording accuracy. This corresponds to a inaccuracy of 0.002-0.003 mm in the recording of the position of the tracers which corresponds in the present case to an error of 1% or less in the high end of the velocity range.

6.2 Results and Discussion

6.2.1 Flow behind a circular cylinder

The technique was first tested in the measurement of the flow behind a cylinder. The frequency of exposures was optimized according to equation 9 and equal to 90 Hz. The exposure time was 1 msec, which corresponded roughly to d_i/V_{max}.

Figure 15 is a triple exposed photograph of the flow. Characteristic fringe patterns, resulting from coherent illumination of selected locations of the photograph are also displayed.

The velocity data was acquired in a regular mesh by digital processing of the Young's fringes, produced by point by point scanning of the photograph. The scanning step size and the dimension of the analyzing beam diameter were .5 mm, which corresponds to a spatial resolution of about 1 mm in the object plane. The fringe patterns were processed using the interactive one-dimensional averaging software described in references 4,6 at the von Karman Institute Digital Image Processing Facility.

Figure 16 shows the mapped two-dimensional velocity vector field superposed on the original photograph. As it can be observed, this data represents with great fidelity the flow field. However, in some regions velocity data drop-out occurs, due to the following reasons. Firstly, at the

locations near the instantaneous centers of rotation of the flow, the velocity of the particles is very close to zero and beyond the low end of the dynamic range of the technique. This could be avoided if the convective flow velocity was measured, for example, by having the camera traveling with the model. Secondly, some data drop-out occurs at random locations due to various reasons such as scratches in the film, fringes with bad SNR or lack of seeding. These regions of signal drop-out were "filled-in" using an interpolation algorithm. Because the two-dimensional velocity field is measured on a square mesh, the spatial derivatives of the velocity, and consequently the vorticity, can be estimated by a simple algorithm. Considering that the grid location of the measurement points are labeled with indices i and j, the vorticity component, $\Omega_{i,j}$, at location i, j is

$$\Omega_{i,j} = \frac{V_{i+1,j} - V_{i-1,j}}{2\Delta x} - \frac{U_{i,j+1} - U_{i,j-1}}{2\Delta y} \qquad (35)$$

For the boundaries of the velocity field, an excentered scheme is used to evaluate the spatial derivatives. This results in a small inaccuracy on the evaluation of the vorticity at the boundary. Figure 17 shows the vorticity contours for the flow behind the cylinder. Improved visualization of the velocity and vorticity fields is obtained by color encoding the different levels of the vorticity component Ω as shown in figure 18.

6.2.2 Flow over the NACA ØØ12 Airfoil

For the flow over the airfoil the frequency of exposures was varied over a wide range from 6Ø Hz to 9Ø Hz. Preliminary analysis of the film negatives showed that best results were obtained with a frequency of 9Ø Hz. The exposure time was 1 msec and kept constant throughout the experiment. Photographs obtained with different number of exposures are shown in figure 19. The figure demonstrates that a significant increase in quality of the "flow visualization" is achieved with a larger number of exposures. Another equally important effect of the number of exposures is the improvement of fringe sharpness and SNR.

A complete analysis of the triple exposed photograph (Figure 19 b)) was also carried out and results are presented on figure 2Ø.

7. CONCLUSIONS

Using the apparatus described in the previous sections a series of Particle Displacement Images were successfully taken using different exposure parameters. Local coherent illumination by the probe laser beam yielded Young's fringes of good quality at almost every location of the flow field. Using the von Karman Institute Image Processing facility, these fringes were analyzed and the velocity and vorticity fields were derived. The present study has lead to the following conclusions:

(i) Particle Image Displacement Velocimetry is indeed suitable for the study of flows with vortical motions.

(ii) In the present study, the flow velocities were limited to a small value (50mm/sec) because of laser power limitations. However this limitation does not apply if a pulsed laser delivering high energy pulses is used. Once a pulsed laser becomes available to us, tests in the FMRL wind tunnel will be conducted to prove the feasibility of the technique in higher velocity (up to 100m/sec) air flows.

(iii) A larger towing tank facility has just become available to the FMRL in which tests can be carried out in a wide range of towing velocities. This facility is provided with camera mounts that travel with the towed model. Therefore it is possible to capture the flow in two reference frames: the one traveling with the model and that of the laboratory.

(iv) The next step in the development of the technique will consist on the development of schemes to compensate for the error introduced by the out-of-plane motion and device methods for its correction. Simultaneously a method for the measurement of the magnitude of the out-of-plane motion will be developed.

(v) The FMRL capabilities in the area of digital processing of the Young's fringes is presently being developed. In a later stage Image Correlation techniques, will also be investigated, and a comparison of the performance of the two methods will be carried out.

References

1. Dimotakis P.E. "Laser measurements in turbulent flow"
   Bull. Amer. Phys. Soc., vol. 28, 1983
2. Wallace J.M. "Measurement of vorticity using hot-wire anemometry"
   Bull. Amer. Phys. Soc., vol. 28, 1983
3. Simpkins P.G., Dudderar T.D. "Laser speckle measurements of transient Bernard convection"
   J. Fluid Mech., vol. 86, 1978
4. Meynart R. "Instantaneous velocity field measurements in unsteady gas flow by speckle velocimetry"
   Applied Optics, vol. 22, 1983
5. Meynart R. "Speckle velocimetry study of a vortex pairing in a low Re unexcited jet"
   Physics of Fluids, vol. 26, 1983
6. Lourenco L.M.M., Meynart R. "Laser speckle velocimetry in fluid dynamics applications"
   in VKI lecture series 1984-Ø3, Digital Image Processing in Fluid Dynamics, 1984
7. Adrian R.J., Yao C.S. "Development of pulsed laser velocimetry (PLV) for the measurement of fluid flow"
   in Proceedings, Eighth Biennial Symposium on Turbulence, Rolla, Mo., 1984
8. Erf R.K. "Application of laser speckle to measurement"
   Laser Applications, vol. 4, Academic Press
9. Elkins R.E., Jackmann G.R., Johnson R.R., Lindgreen E.R., Yoo J.K. "Evaluation of stereoscopic trace particle records of turbulent flows"
   Rev. Sci. Instrum., vol. 48, 1977
10. Yao C.S., Adrian R.J. "Orthogonal compression and one-dimensional analysis technique for measurement of two-dimensional particle displacements in pulsed laser velocimetry"
    Applied Optics, vol. 23, 1984
11. Lourenco L.M.M. "Velocity measurement by optical and digital processing of time exposed particle images"
    Bull. Amer. Phys. Soc., vol. 29, 1984
12. Adrian R.J. "Scattering particle characteristics and their effect on pulsed laser measurements of fluid flow: speckle velocimetry vs. particle image velocimetry"
    Applied Optics, vol. 23, 1984

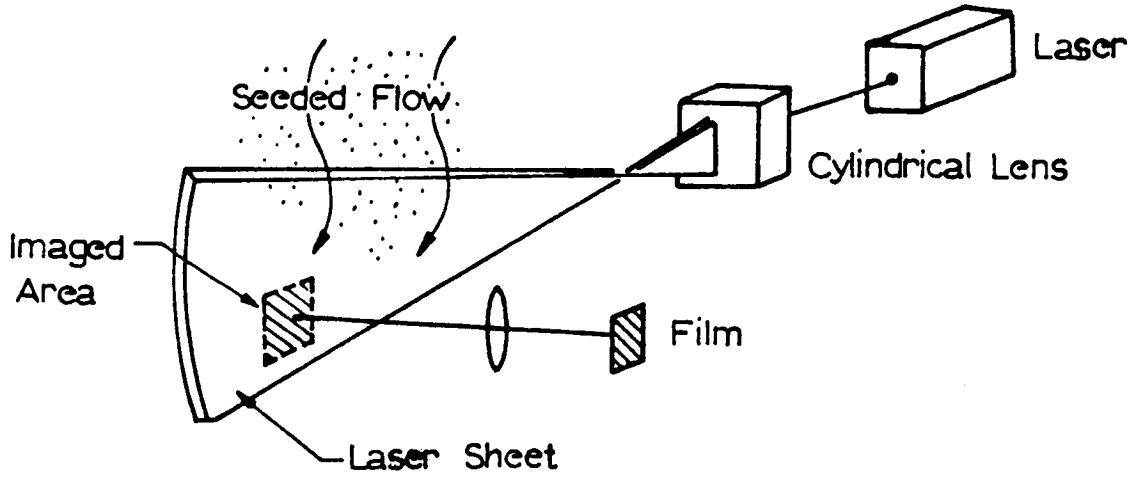

Figure 1. Schematic of an arrangement for photography

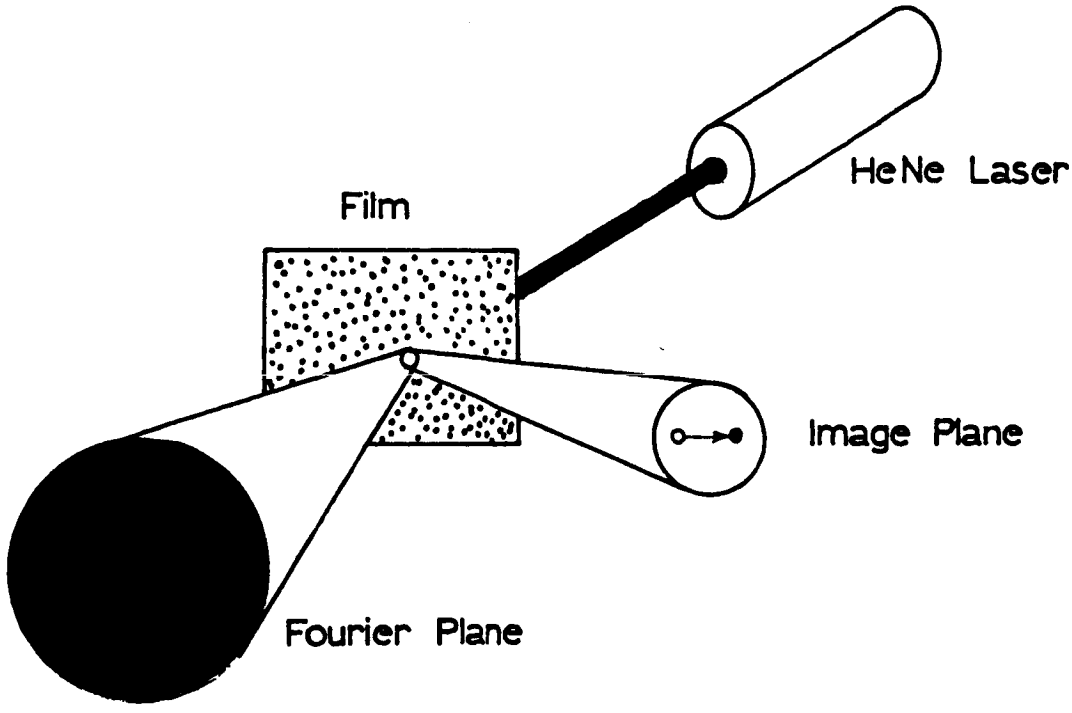

Figure 2. Young's fringe pattern generated by a particle pair.

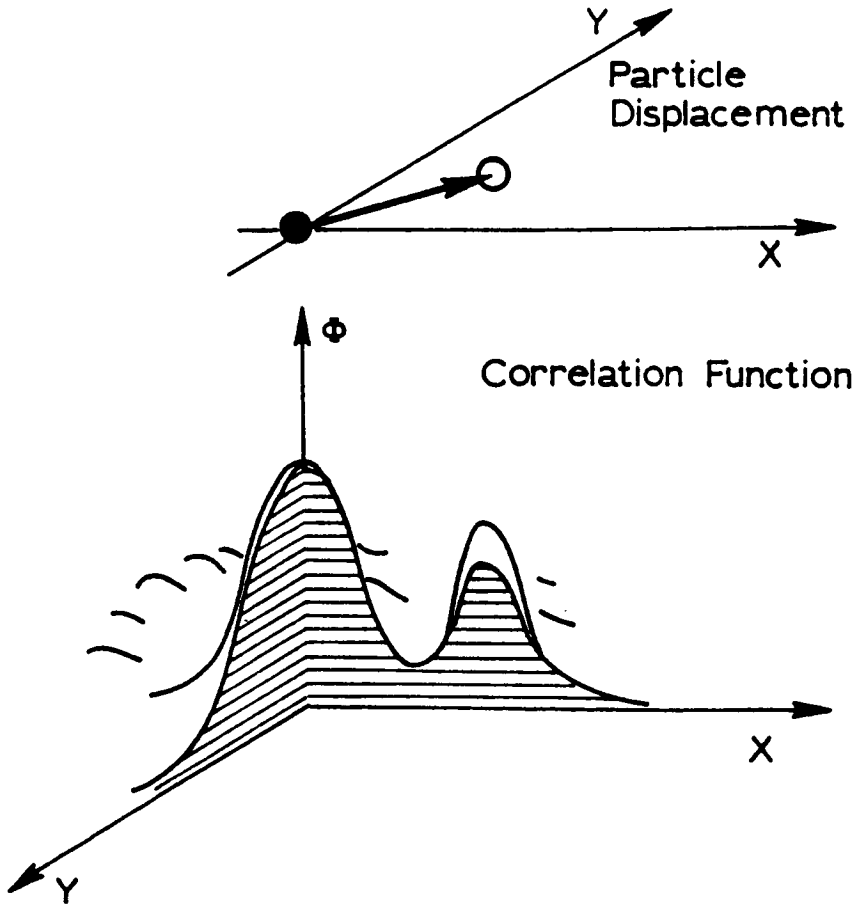

Figure 3. Schematic of the image correlation function

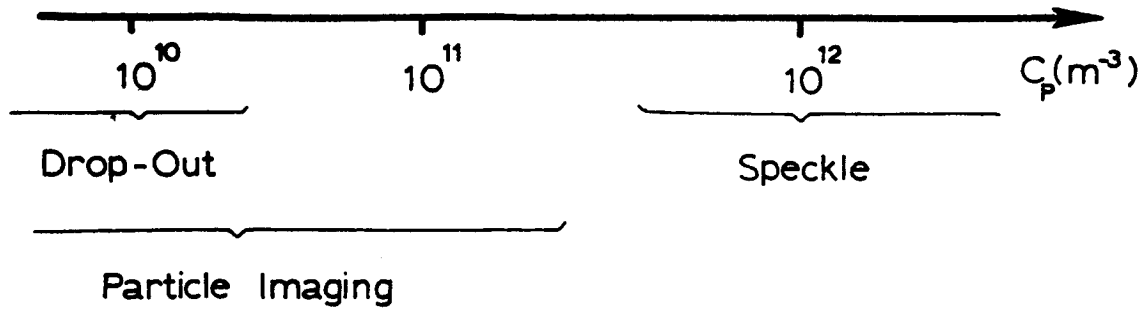

Figure 4. Mode of operation versus seeding concentration

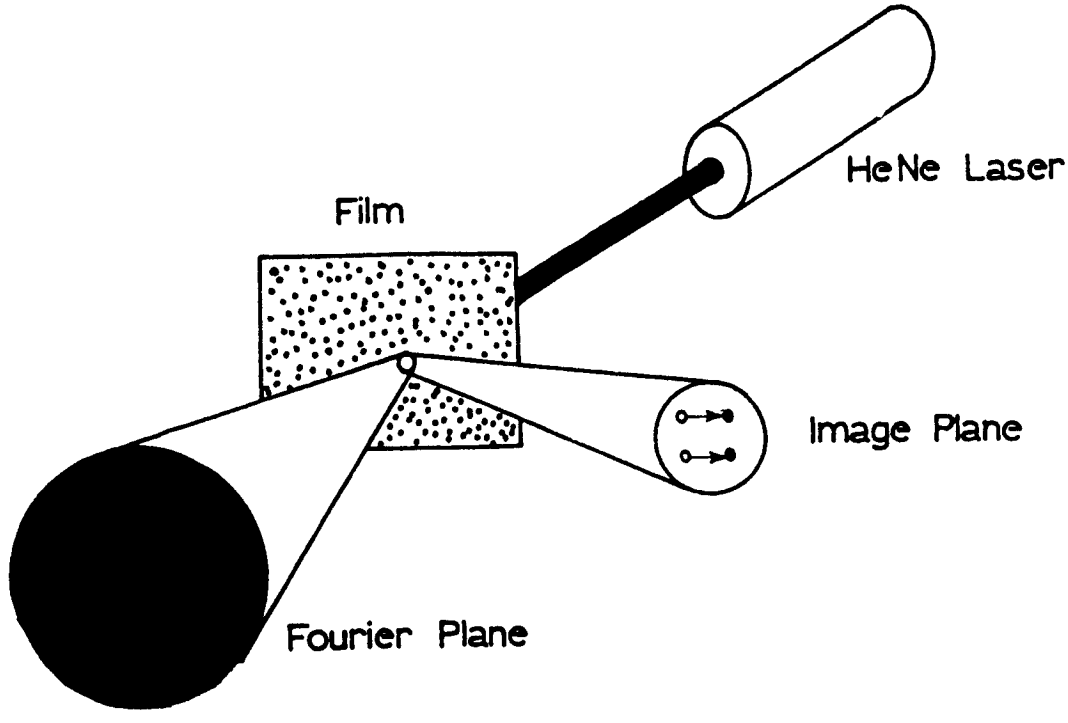

Figure 5. Cross-interference fringe pattern generated by two particle pairs.

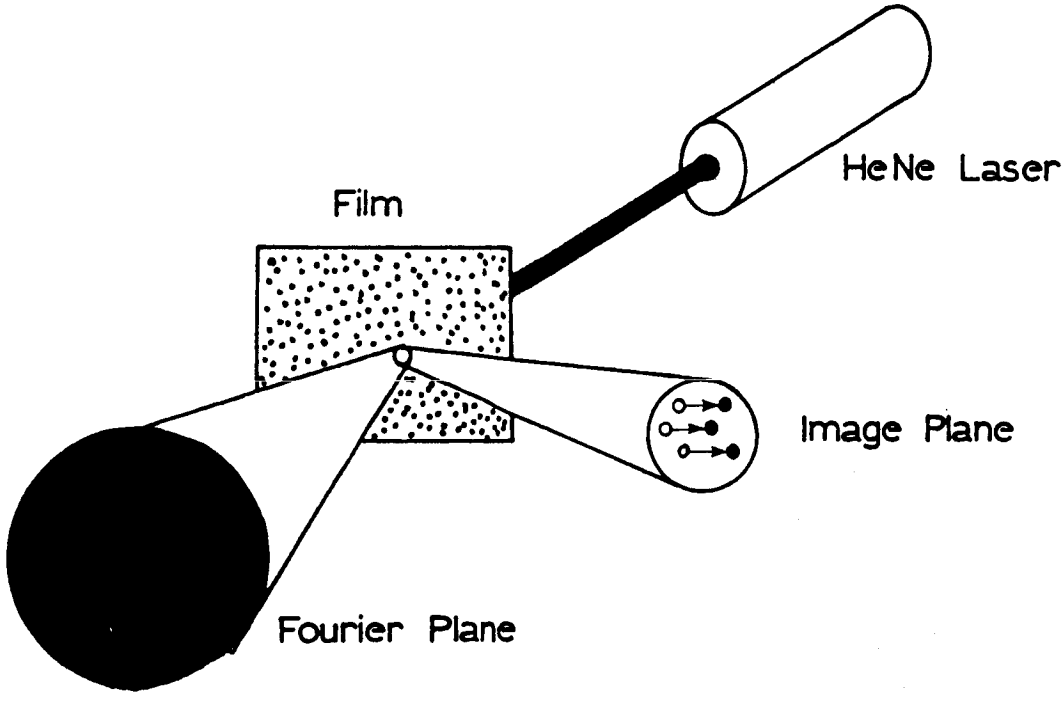

Figure 6. Fringe pattern generated by multiple image pairs.

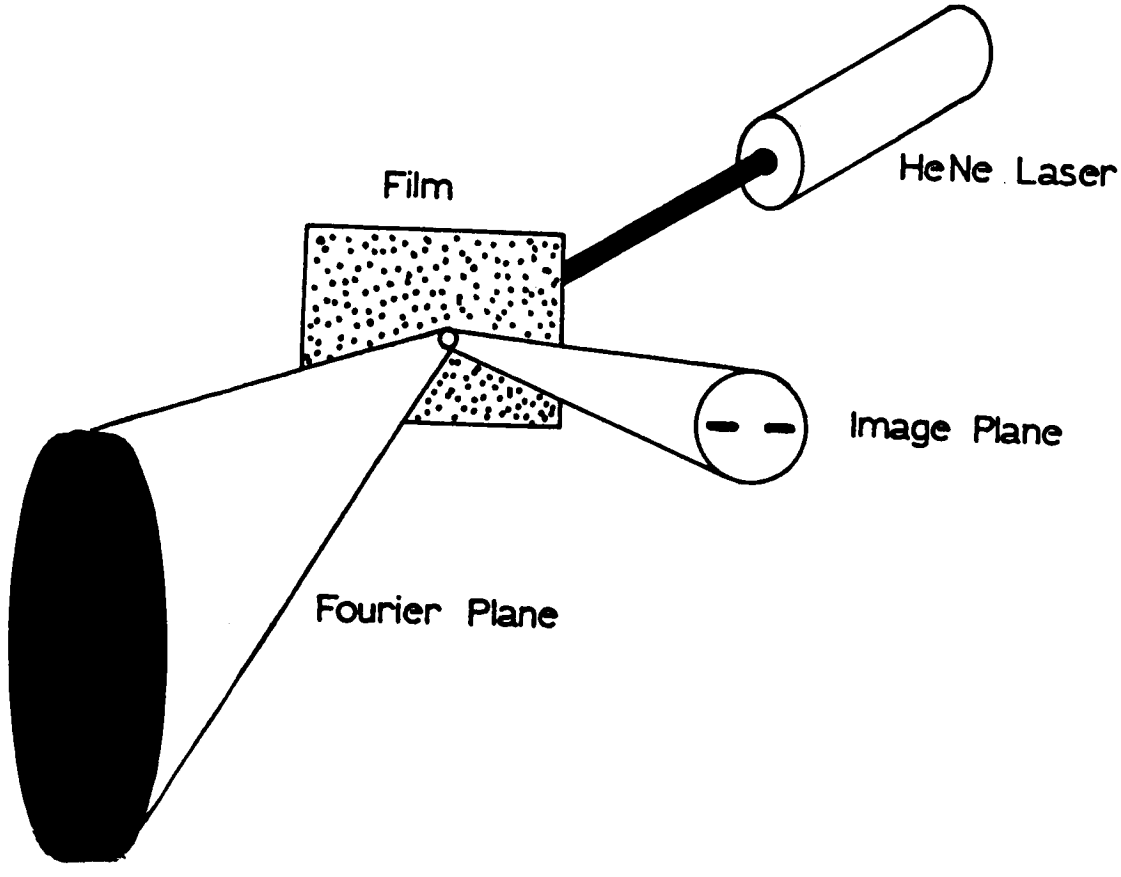

Figure 7. Fringe pattern generated by streak images.

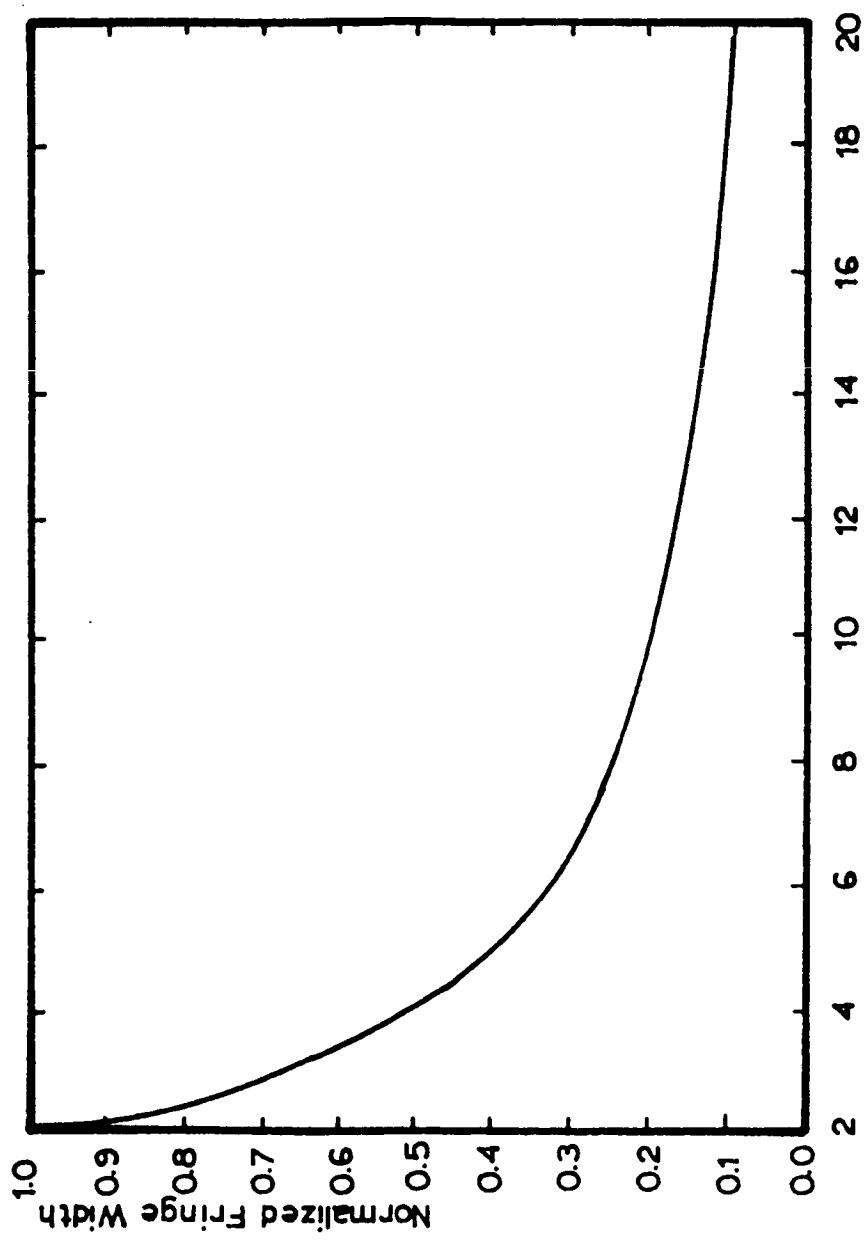

Figure 8. The variation of fringe width with number of exposures.

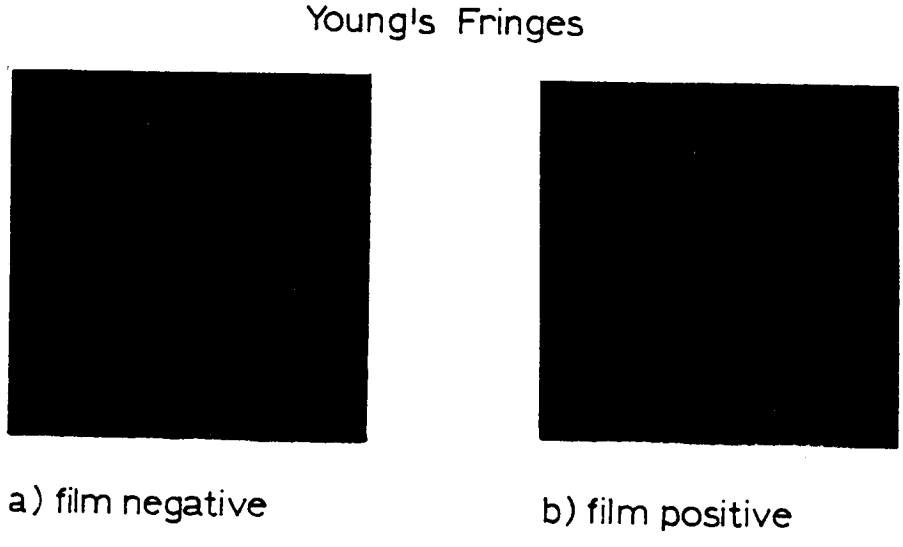

Figure 9. Young's fringe patterns obtained with film negative and positive.

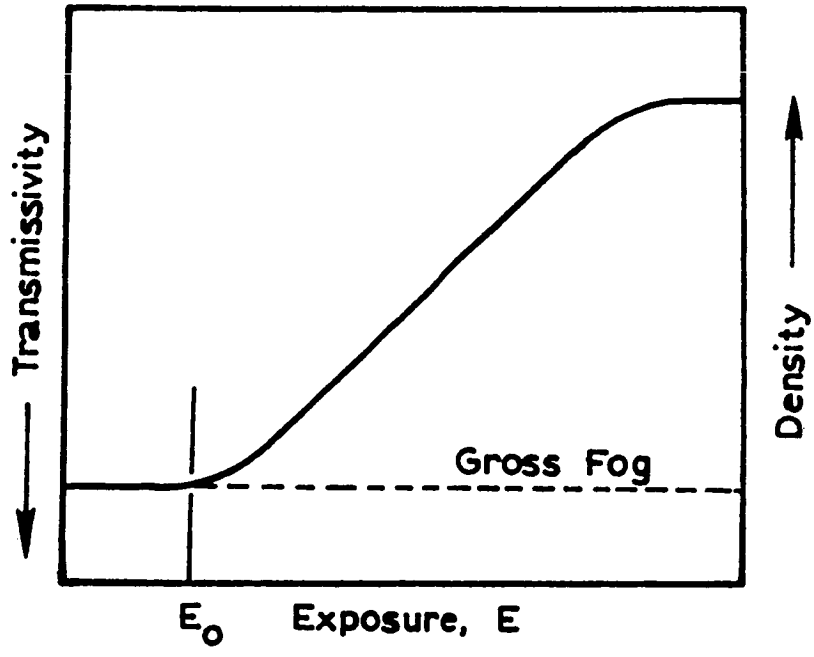

Figure 10. The density-exposure curve for a film

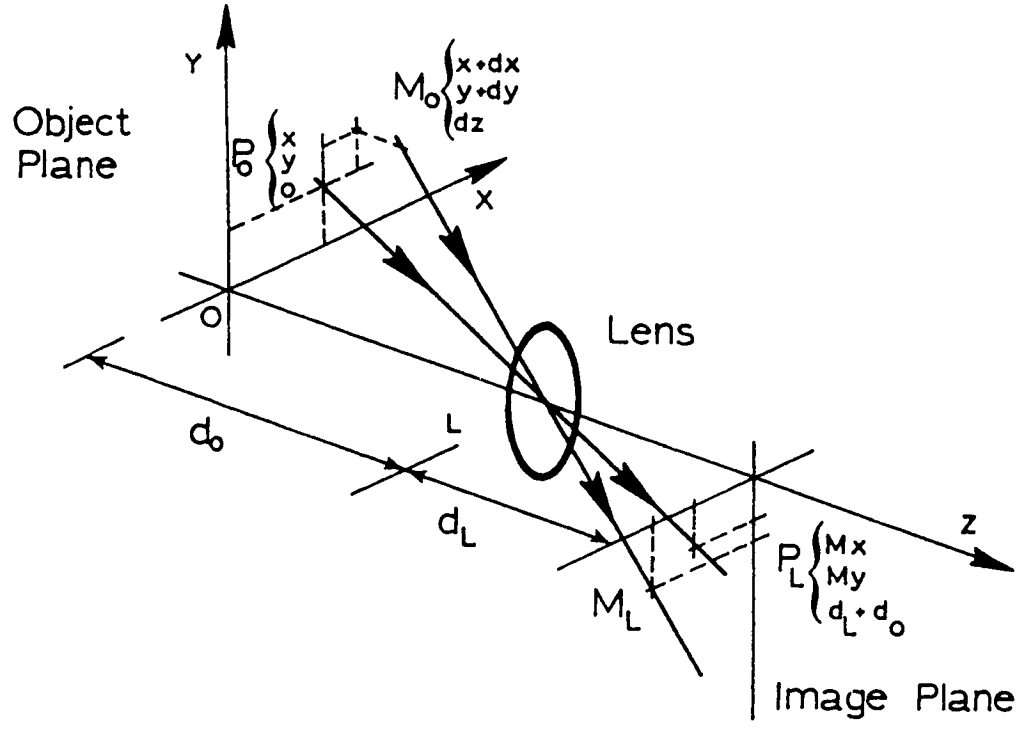

Figure 11. A schematic of the imaging system for the estimation of the out-of-plane motion.

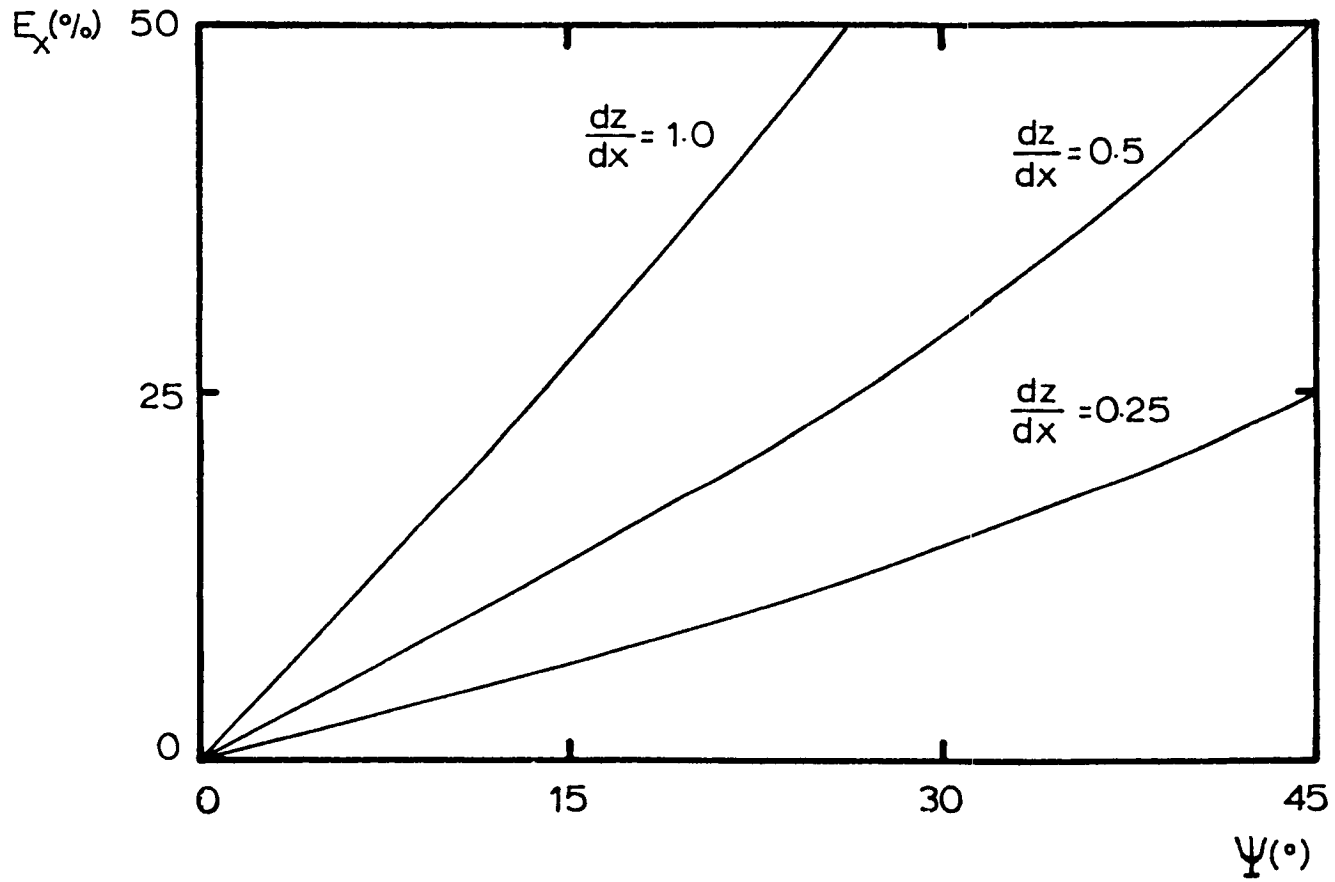

Figure 12. Theoretical relative error of in-plane component due to out-of-plane motion.

Figure 13. Photograph of the experimental facility.

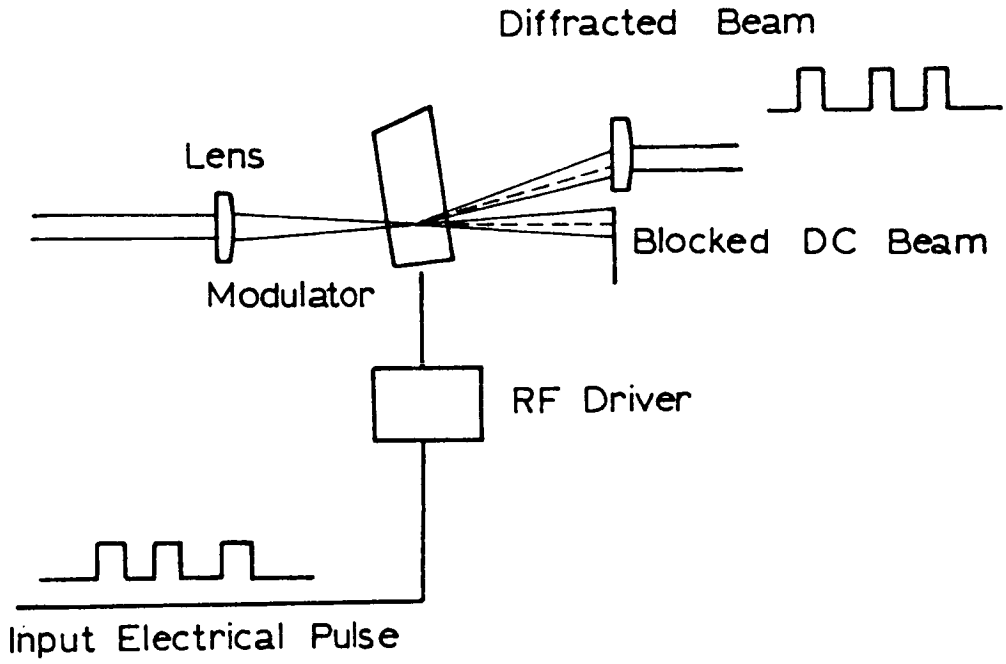

Figure 14. Schematic of the laser shutter

Figure 15. Triple exposed photograph of the vortex street.

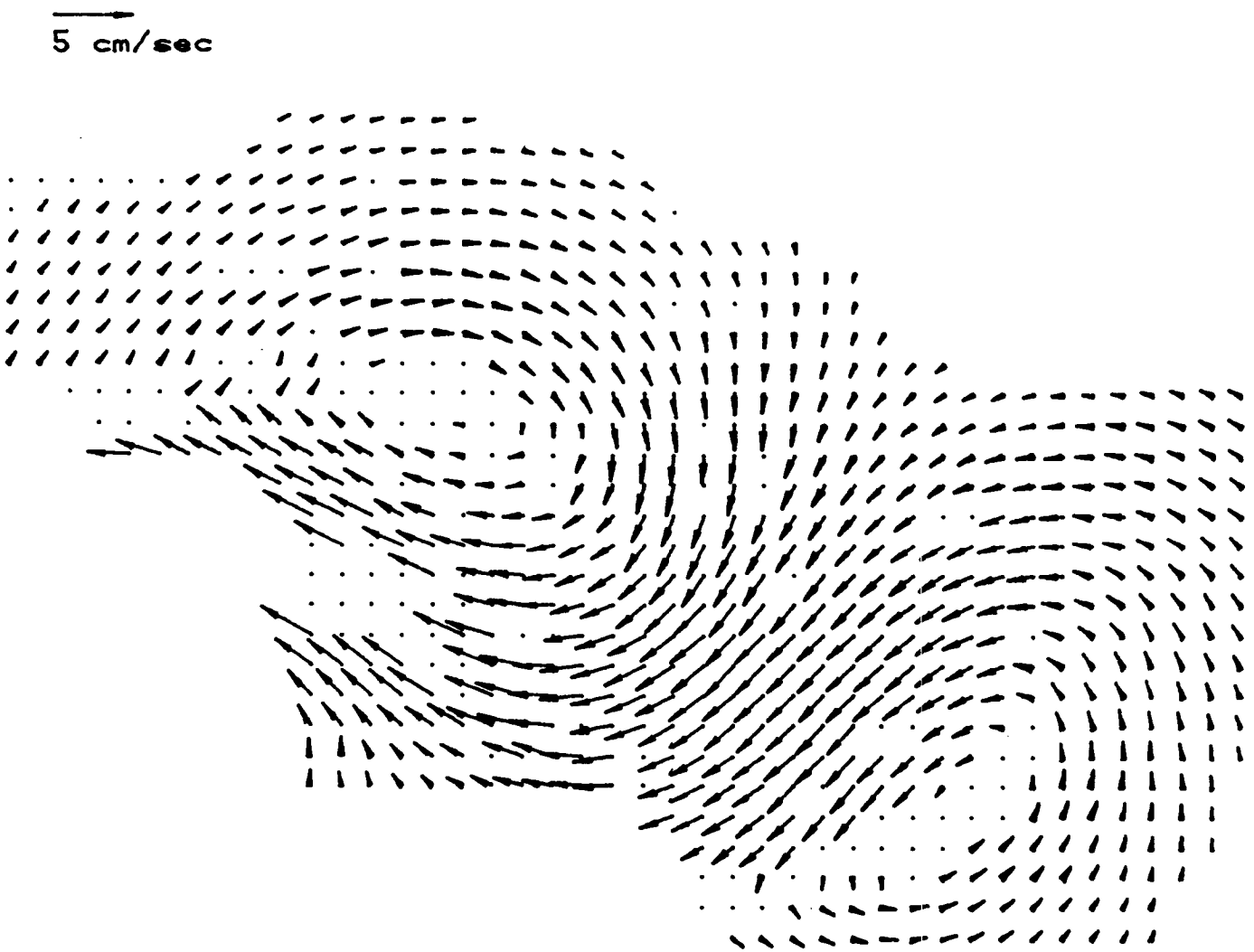

Figure 16. Velocity vector map of the vortex street

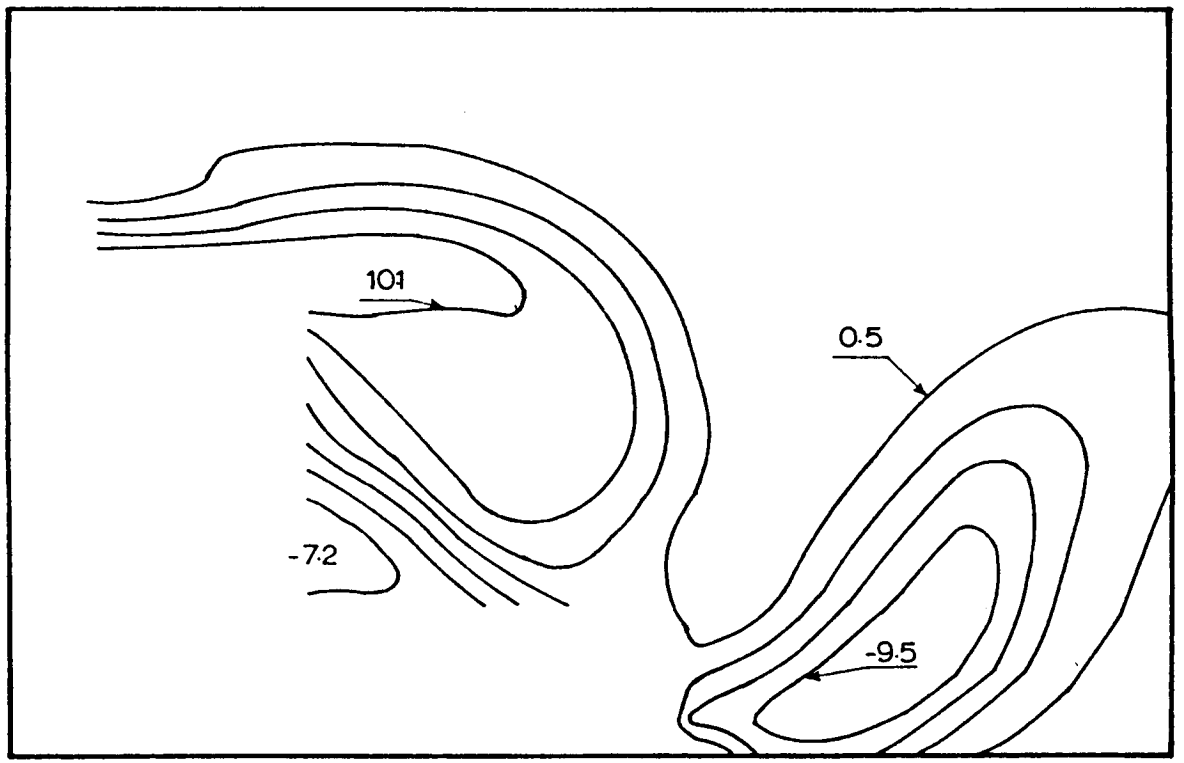

Figure 17. Constant vorticity contours of the vortex street.

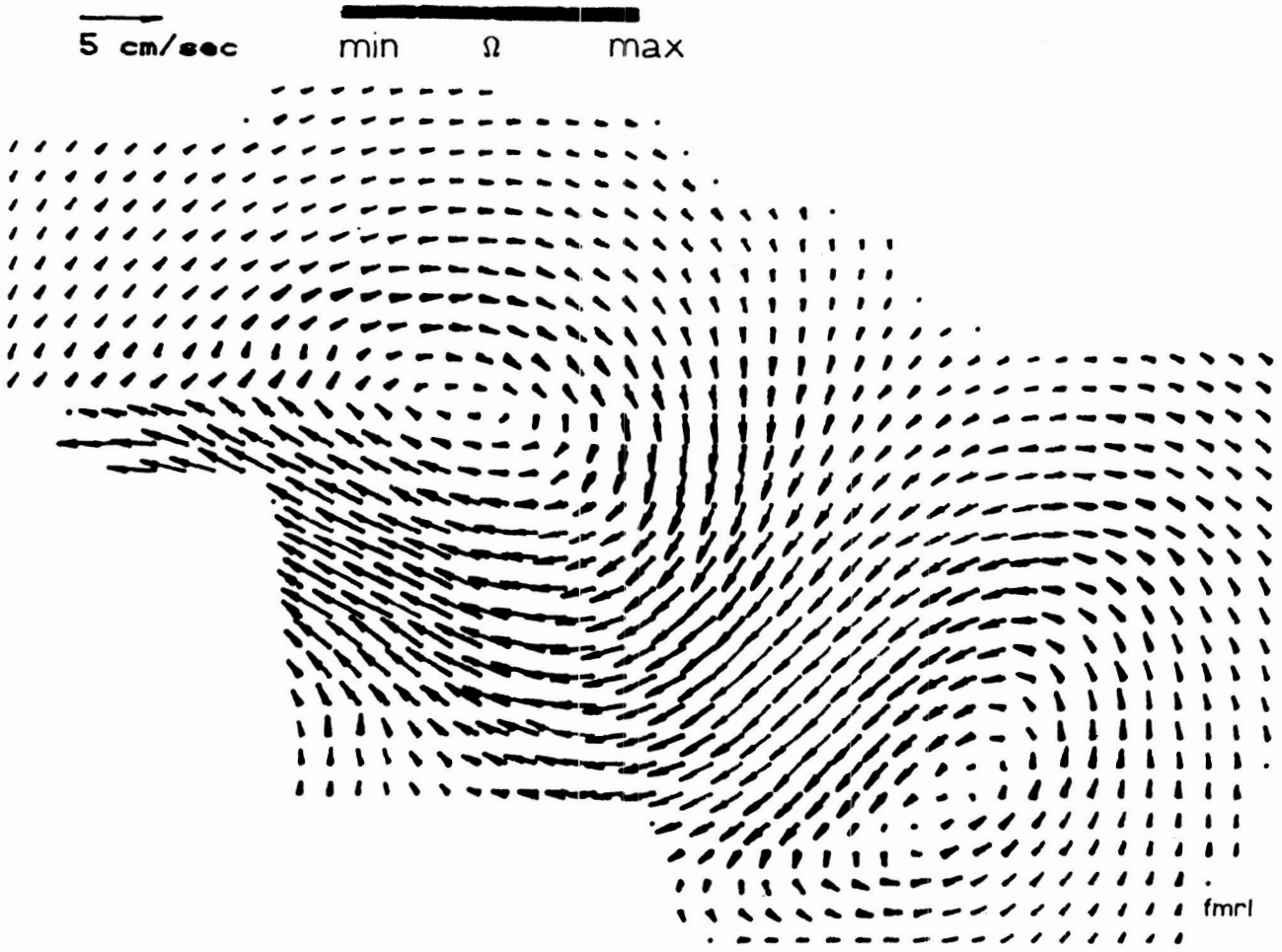

Figure 18. Velocity and vorticity fields of the Karman vortex street.

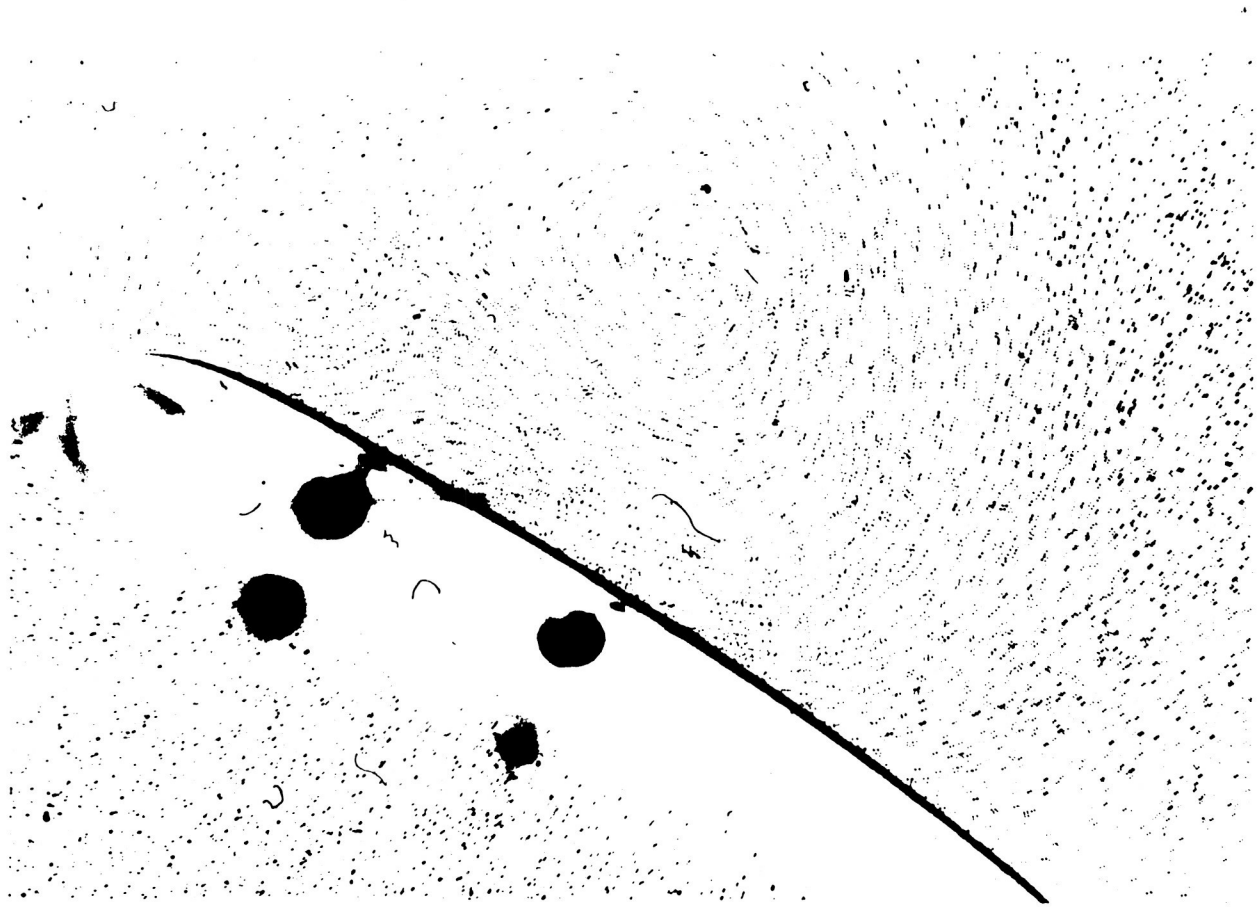

Figure 19a. For legend see figure 19c.

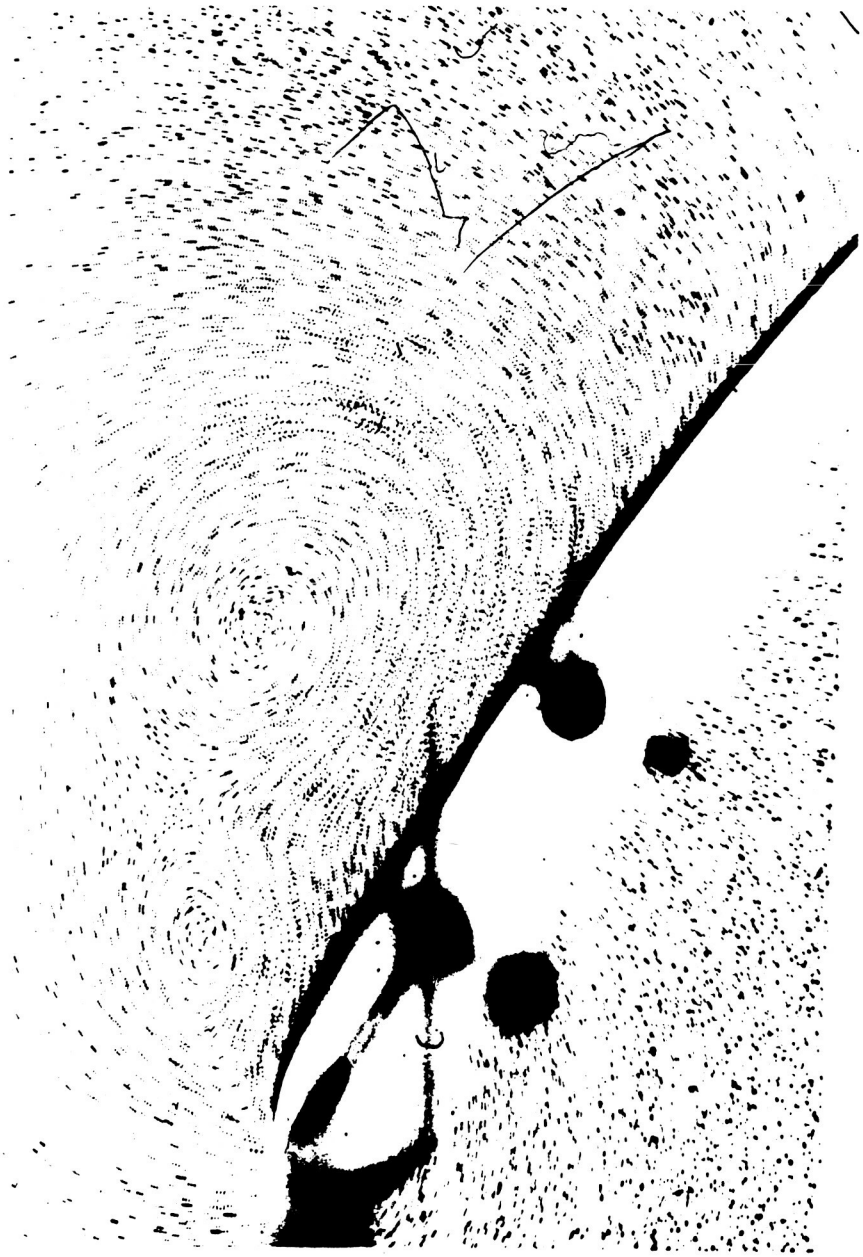

Figure 19b. For legend see figure 19c.

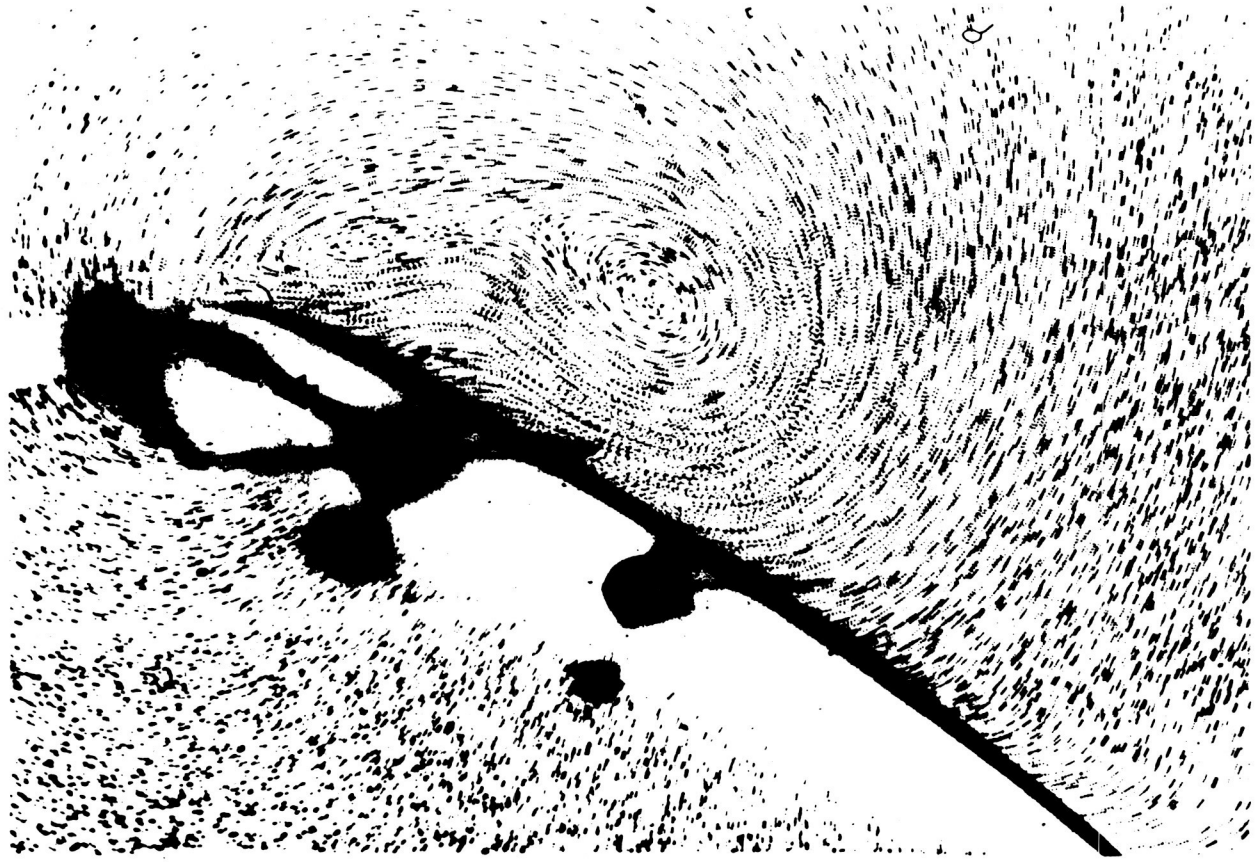

Figure 19c. Multiple exposure photographs of flow past an airfoil at 30 degrees angle of incidence; a) double exposure, b) triple exposure, c) Quadruple exposure.

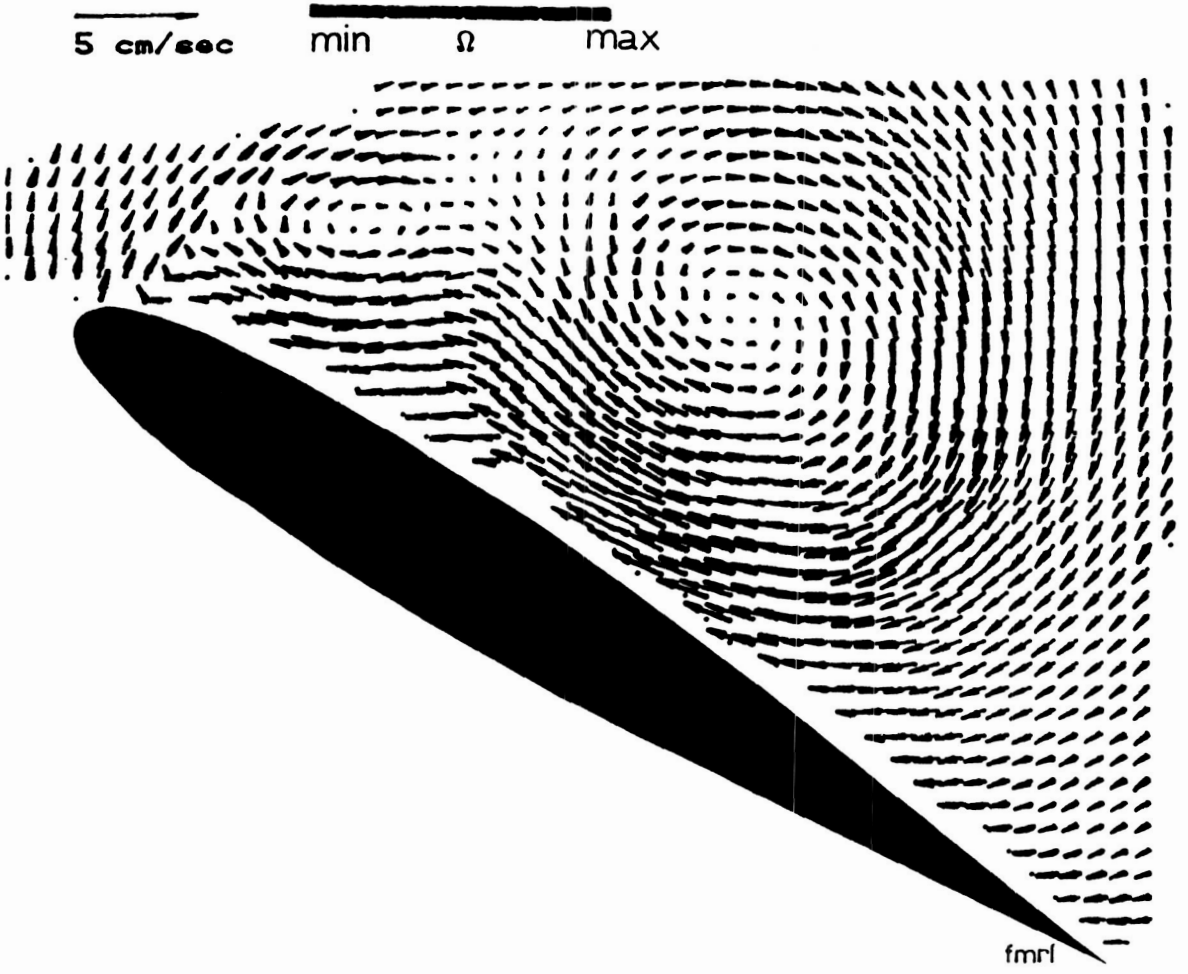

Figure 20. Velocity and vorticity fields of flow over a NACA 0012 airfoil.